Estimation of Local Equilibrium Model Parameters for Simulation of the Laboratory Foam-Enhanced Oil Recovery Process Using a Commercial Reservoir Simulator

Lei Ding,* Leyu Cui,* Stephane Jouenne, Oussama Gharbi, Mayur Pal, Henri Bertin, Mohammad Azizur Rahman, Carolina Romero, and Dominique Guérillot*

ACCESS | 📊 Metrics & More | 📖 Article Recommendations | 🔳 Supporting Information

ABSTRACT: An accurate determination of the foam simulation parameters is crucial in modeling foam flow in porous media. In this paper, we present an integrated workflow to obtain the parameters in the local equilibrium foam model by history matching a series of laboratory experiments performed at reservoir conditions (131 F and 1500 psi) on Estaillades limestone using a commercial reservoir simulator. The gas−water and water−oil relative permeability curves were first validated after history matching with the unsteady-state flooding experiments. The modeling parameters for foam generation and foam dry-out effect were obtained by history matching with the gas/surfactant coinjection experiments at varying foam quality and injection rates. Moreover, the modeling parameters for the destabilizing effect of oil on foam and foam shear thinning effect were derived after history matching with the foam-enhanced oil recovery process and oil fractional flow experiments in the laboratory. In practice, the calculated results reproduce the experimental outputs reasonably well. Furthermore, sensitivity analysis of foam modeling parameters is investigated to determine the most dominating parameters for accurate simulation of foam-enhanced oil recovery process in porous media. In this work, an efficient parameter estimation approach is developed from reliable foam flooding experimental data, which may be further applied to field-scale simulation. Moreover, the simulation approach can also be utilized to facilitate our interpretation of complex lab foam flooding results.
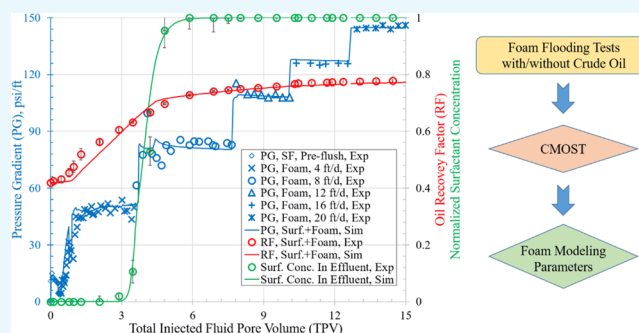
1. INTRODUCTION

Foam has been widely used for mobility control and conformance to improve oil recovery in oil reservoirs, and it could efficiently address challenges related to gas flooding, such as viscosity fingering, gravity segregation, and gas channeling.[1−3] Foam flow in porous media is inherently a dynamic process of lamellae generation and lamellae coalescence.[4] Lamellae could be readily generated in situ in porous media through snap-off,[5,6] lamellae division,[7−9] and leave-behind[10] while it could also easily collapse because of gas diffusion, gravity drainage, and capillary suction.[11,12]

Two distinct regimes, namely low-quality regime and high quality regime, have been observed in the strong foam state.[13−15] In the high-quality regime, the foam strength is almost independent of gas superficial velocity, and the foam behavior is controlled by limiting capillary pressure[16,17] while in the low-quality regime, the foam strength is independent of water superficial velocity and it is dominated by yield stress as well as bubble train mobilization. The other important finding is that there exists a minimum pressure gradient (MPG) for strong foam to be readily generated in homogeneous porous media, and

it may occasionally be referred as a critical superficial velocity in some literature.[18,19]

Foam can largely reduce the mobility of gas in two aspects: one is to decrease the gas relative permeability and the other is to increase the gas apparent viscosity.[11,20] Interestingly, it has been proved experimentally that the relative mobility to water at a given water saturation is not directly influenced by the presence of foam.[21,22] Therefore, the most commonly used two-phase flow (gas and aqueous phases) foam models only address the reduction in gas mobility.[23]

There are generally two approaches for modeling foam flow in porous media, that is, texture explicit population balance (PB) model and texture implicit local equilibrium (LE) foam model.[24,25] The PB model requires solving an additional partial

differential equation for conservation of bubble population with exact expressions to describe lamellae generation and destruction.[26] The PB model has clear physics, but it is generally not viable to be applied to large-scale reservoir simulation because of its expensive computational cost. Moreover, there are more adjustable parameters in the PB model, of which some kinematic parameters in foam generation and foam coalescence functions are extremely difficult to be obtained.[24,27]

Comparatively, the LE model uses only an empirical algebraic formula to correlate the gas mobility reduction with certain local conditions.[23] Numerous results have shown that the characteristic time for foam generation and coalescence is much shorter than that for foam transport, therefore it is justifiable to assume that the rates of lamellae generation and coalescence are locally at the equilibrium state.[24] Although there is no explicit foam generation and coalescence function, the physics of foam behavior in porous media is reported to be equally honored in the LE model.[28,29] However, it has been acknowledged that the LE model is not capable of capturing transient foam behavior and capillary entrance effect.[4,23]

Among many available LE foam models, for example, UTCHEM,[30] ECLIPSE,[31] STARS/GEM,[32] PUMA,[33] MoReS,[34,35] AD-GPRS,[24] and so forth, the most widely used LE foam model is the STARS model developed by the Computer Modeling Group (CMG). In this model, the gas relative permeability in the presence of foam is calculated by multiplying a dimensionless interpolated factor (FM) with the gas relative permeability in the absence of foam.[23,36] FM can be calculated as a function of different variables, for example, surfactant concentration, oil saturation, salinity, oil composition, capillary number, permeability, water saturation, and so forth.[37−39]

The surfactant concentration effect (F_1),[40,41] oil saturation effect (F_2),[33] shear thinning effect (F_3),[10,42−44] foam generation effect (F_4),[30] oil composition effect (F_5), salinity effect (F_6),[45] permeability effect (F_7),[44] and foam dry-out effect (F_{dry})[2,10] have been investigated elaborately in the LE foam model. Selected literatures related to foam flow modeling using the STARS LE foam model are summarized in Table 1. The detailed description of $F_1−F_{dry}$ functions is found in the Supporting Information (S2).

An accurate determination of foam simulation parameters is crucial in modeling foam flow in porous media. However, it requires extensive and reliable experimental work. Moreover, the existence of nonuniqueness or nonphysical solutions also jeopardizes the foam modeling process. In this paper, we present an integrated workflow to obtain the physical modeling parameters in the LE foam model by history matching a series of laboratory experiments using CMG STARS and CMOST.

2. MATERIALS AND METHODS

2.1. Experimental Section. *2.1.1. Instruments.* All the flooding experiments were performed on Grace M9300 core flooding setup from Grace Instruments, which combines a core flow tester with a foam rheometer and can be performed at high temperature, elevated pressure, and high salinity/hardness reservoir conditions. The confining pressure and backpressure can be precisely controlled at a wide range of reservoir pressure. A schematic diagram for the foam coinjection process, that is, coinjection of nitrogen and surfactant solution, is listed in Figure 1.

The surfactant solution and gas were coinjected into the core from the bottom during experiments, which is, yet, essentially

**Table 1. Summary of Foam Modeling Literatures Using the STARS LE Model**

references	F_1	F_2	F_3	F_4	F_5	F_6	F_7	F_{dry}
Abbaszadeh, 2018[42]			√					√
AlMaqbali, 2015[38]			√					√
Aydin, 2019[32]	√	√	√					
Cui, 2016[45]						√		√
Farajzadeh, 2015[16]							√	√
Hosseini-Nasab, 2018[33]	√	√	√					√
Jian, 2019[46]	√	√	√					√
Kahrobaei, 2017[40]	√							√
Kahrobaei, 2019[41]	√							√
Kapetas, 2015[43]			√					√
Kapetas, 2016[44]			√					√
Lottashi, 2017[30]				√				
Ma, 2013[2]								√
Ren, 2019[39]	√	√						√
Spirov, 2015[31]	√	√	√					√
Tang, 2019[47]	√	√	√					√
Zeng, 2019[34]	√	√						√
Zeng, 2020[35]	√	√						√

not a favorable process for gas injection. However, this effect may be not severe at the core scale in this study. Moreover, this injection scheme may also be occurred in the field, which can also be optimized by reservoir simulation. The mass of effluent is recorded automatically using an electrical precision balance (My Weigh iM01) to calculate the water saturation in the core sample after foam flooding. The surfactant concentration in the effluent aqueous phase was analyzed by high-performance liquid chromatography (HPLC, Alliance Waters). The surface tension of surfactant solution and the interfacial tension (IFT) between oil and surfactant solution are measured by the shape analysis method (by Ramé-Hart model 500 Goniometer).

2.1.2. Material Chemicals. The core sample is Estaillades limestone from outcrop. The surfactant is $C_{8−16}$ alkyl polyglucoside (APG) from BASF (lot no. Aspiro S2410X), and the gas is N_2. The ISCO pump is used for injection of nitrogen. The required gas flow rate at room temperature (77 F) for attaining desired foam quality at reservoir conditions can be calculated by applying the ideal gas law. The specification of core samples and chemicals is listed in Table 2.

2.1.3. Procedures. The experiments were all conducted at 2000 psi confining pressure and 1500 psi back pressure at 131 F, unless otherwise specified. The synthetic injection seawater brine for water flooding (WF) and surfactant flooding is approximately 44,000 total dissolved solids (TDS), and the synthetic formation brine is approximately 150,000 TDS. The foam quality in porous media tests is defined as the gas fractional flow at reservoir conditions ($f_g = u_g/u_g + u_l = u_g/u_t$), where u_g, u_l, and u_t are gas, liquid, and total superficial velocity, respectively. After each foam test (without crude oil), the core is restored before reutilized. In this study, steady-state foam behavior refers to the state during the coinjection (of surfactant solution and gas) process after the pressure gradient (PG) across the core is fairly stable,[48] that is, the fluctuations in pressure drop are within 5% of its averaged value in a period of 2.0 total pore volume (TPV). A detailed procedure is elucidated in S1 in the Supporting Information.

2.2. Numerical Simulation Section. A one-dimensional LE foam model is developed, and the data file can be found in the Supporting Information (S4). The capillary pressure and
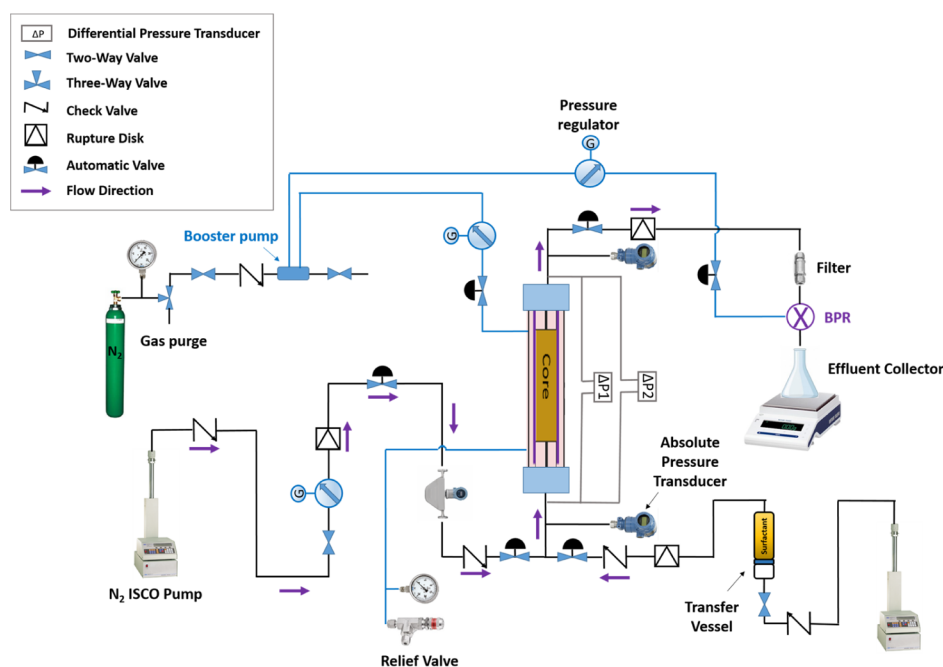
ΔP1: 0-20 psi; ΔP2: 0-200 psi

Figure 1. Schematic diagram of the Grace M9300 core flooding apparatus for proposed nitrogen/surfactant solution coinjection process.

Table 2. Core Samples and Chemicals for Foam Tests

core sample (Estaillades limestone)				chemicals
length	diameter	permeability	PV	surfactant solution
15.24 cm	3.84 cm	150 ± 2 mD	54 mL	0.20 wt % C_{8-16} APG in synthetic seawater brine

surfactant partition into oil are assumed to be negligible. If the capillary pressure functions are readily available, one may also include the capillary pressure into the model. The surfactant effect (F_1), oil effect (F_2), capillary number (shear thinning, F_3, and generation, F_4), and foam dry-out effect (F_{dry}) are investigated in the modeling of foam flow in this study.

2.2.1. Reservoir Model. A simple one-dimensional, homogeneous, and vertical reservoir model with 50 grid blocks is built. The key parameters of this reservoir model and fluid properties are listed in Table 3. There are two injection wells at the bottom, one of which for liquid injection "INJ-W" and the other for gas injection "INJ-G", and a production well "PROD" at the top.

2.2.2. LE Foam Model in STARS. Due to the fact that the relative permeability and viscosity are always coupled in the flow equations, the STARS LE model only modifies the gas relative

Table 3. Reservoir Model and Fluid Properties

parameters	value	parameters	value
grid blocks	$1 \times 1 \times 50$	end point water relative permeability	0.24
cross section	11.34 cm^2	end point oil relative permeability	0.81
core length	15.24 cm	oil density at 131 F	0.90 g/cm^3
porosity	0.312	oil viscosity at 131 F	40.6 cP
permeability	150 mD	water viscosity at 131 F	0.53 cP
temperature	131 F	gas viscosity at 131 F	0.04 cP
pressure	1500 psi	injection direction	upward

permeability in the presence of foam. In this model, the gas relative permeability in the presence of foam is calculated by multiplying a dimensionless interpolated factor (FM) with the gas relative permeability in the absence of foam (eqs 1 and 2). The mathematical description of F_1–F_{dry} functions in FM and the influence of different parameters on F_1–F_{dry} are summarized in S2 in the Supporting Information.

$$k_{rg}^{f} = k_{rg}^{nf} \times \text{FM} \tag{1}$$

$$\text{FM} = \frac{1}{1 + \text{FMMOB} \times F_1 \times F_2 \times F_3 \times F_4 \times F_{dry}} \tag{2}$$

In this paper, we will mainly consider the effect of surfactant concentration (F_1), oil saturation (F_2), capillary number (shear thinning, F_3, as well as generation, F_4), and water saturation (i.e., foam dry-out effect, F_{dry}). These different factors are summarized by eqs 3–7. These functions are all in the range of $[0-1]$, and the closer they are to unity, the more efficient the foam will be.

$$F_1 = \begin{cases} 1, & \text{if } C_{surf} \geq \text{fmsurf} \\ (C_{surf}/\text{fmsurf})^{\text{epsurf}}, & \text{if } C_{surf} < \text{fmsurf} \end{cases} \tag{3}$$

where C_{surf} is the surfactant concentration, fmsurf is the reference surfactant concentration above which foam strength is independent of the surfactant concentration, and epsurf is the exponent that controls the stiffness of foam strength as a function of surfactant concentration, as illustrated in Figures S1a and S2 in the Supporting Information.

$$F_2 = \begin{cases} 1, & \text{if } S_o \leq \text{floil} \\ 0, & \text{if } S_o \geq \text{fmoil} \\ \left(\dfrac{\text{fmoil} - S_o}{\text{fmoil} - \text{floil}}\right)^{\text{epoil}}, & \text{otherwise} \end{cases} \tag{4}$$

where floil is the lower limit of oil saturation below which foam strength is not affected, fmoil is the critical oil saturation that foam starts to completely collapsed, and epoil is the exponent that regulates the sharpness of foam decay by oil saturation, as illustrated in Figures S1b and S3 in the Supporting Information.

$$F_3 = \begin{cases} 1, & \text{if } N_{ca} \leq \text{fmcap} \\ (\text{fmcap}/N_{ca})^{\text{epcap}}, & \text{if } N_{ca} > \text{fmcap} \end{cases} \quad (5)$$

where N_{ca} is the local capillary number, a dimension-less quantity representing relative effect of viscous force versus interfacial force, $N_{ca} = v\mu/\sigma$, where v is the interstitial velocity of injected fluid, μ is the dynamic viscosity of injected fluid, and σ is the surface/IFT between injected and displaced fluids. In terms of foam flooding, μ is taken as the foam apparent viscosity (μ_{app}). In this study, it is regarded that the injected fluid is gas, and the displaced fluid is water for surface tension and capillary number calculation. In practice, the capillary number is calculated by $N_{ca} = k_{rock}\nabla p/\sigma$ in the simulator, where k_{rock} is the absolute permeability and ∇p is the PG. In eq 5, fmcap is the critical capillary number above which non-Newtonian foam behavior is expected. Foam is a shear thinning fluid if epcap is positive, as illustrated in Figures S1c and S4 in the Supporting Information.

$$F_4 = \begin{cases} 0, & \text{if } N_{ca} \leq \text{fmgcp} \\ (\text{fmgcp} - N_{ca}/\text{fmgcp})^{\text{epgcp}}, & \text{if } N_{ca} > \text{fmgcp} \end{cases} \quad (6)$$

where fmgcp is the reference capillary number above which foam can be readily generated, and epgcp is the exponent. A demonstration of the effect of these parameters is shown in Figure S1d in the Supporting Information.

$$F_{dry} = 0.5 + \frac{\arctan[\text{sfbet} \times (S_w - \text{SFDRY})]}{\pi} \quad (7)$$

SFDRY is the limiting water saturation, below which the foam is getting unstable and the foam dry-out effect starts dominating the foam behavior. It can be calculated as a function of surfactant concentration, oil saturation, salinity, and capillary number in the new version of CMG STARS (CMG, 2017 or later). However, we will treat SFDRY as a fixed value in this paper. The physical interpretation of other parameters is elucidated in nomenclature and in S2 in the Supporting Information. sfbet regulates the slope of F_{dry} near SFDRY, that is, the abruptness of foam dry out effect, as illustrated in Figure S1h in the Supporting Information.

The flowchart for history matching the lab experimental results is elucidated in Figure 2. The largest uncertainty for flow simulation may be the relative permeability curve. In this paper, the relative permeability curves are obtained from the literature with small adjustment by history matching the process of unsteady-state flooding tests in the laboratory.

Then, the foam generation (F_4) and foam dry-out (F_{dry}) functions in the STARS LE foam model are obtained after history matching the foam coinjection experiments in the absence of oil at reservoir conditions. Furthermore, the modeling parameters for oil destabilization effect (fmoil, floil and epoil) and foam shear thinning effect shear thinning effect (fmcap and epcap) are derived by history matching the foam-enhanced oil recovery (EOR) and oil fractional flow experiments in the laboratory. CMOST is a very useful tool in history matching, sensitivity analysis, uncertainty analysis, and optimization and is utilized for history matching in this paper.
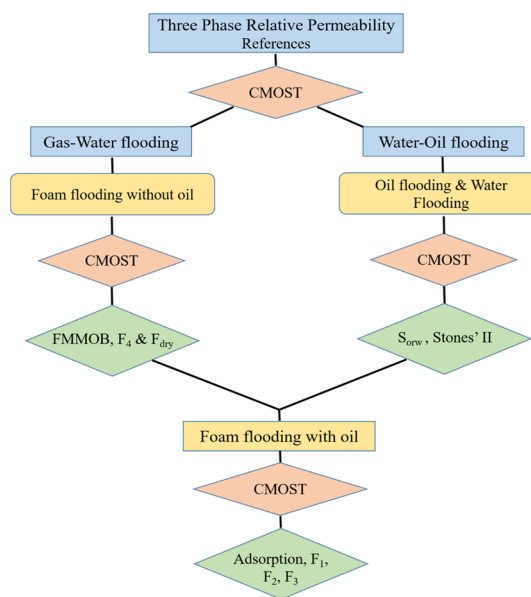

Figure 2. Flow chart for obtaining LE foam modeling parameters.

3. RESULTS AND DISCUSSION

3.1. Simulation of Foam Transport in Porous Media in the Absence of Crude Oil. *3.1.1. Simulation of Continuous Gas Injection Process.* The gas–water two-phase relative permeability curve was first validated by history matching the process of continuous gas injection (CGI) into the 100% synthetic seawater brine saturated porous medium. The gas–water relative permeability curve is assumed to follow Corey's model,[49] and the mathematical description is found in the Supporting Information (S3). The effect of surfactant on gas–water two-phase relative permeability is assumed to be negligible. Figure 3 discloses the PG across the core holder
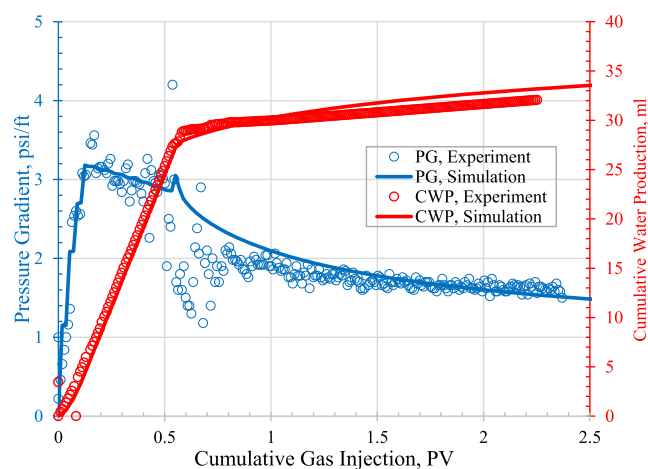

Figure 3. PG and cumulative water production during the CGI process at 4 ft/d for both simulations (solid lines) and experimental measurements (points).

and water production during the CGI process at 4 ft/d, and Table 4 summarizes the key values for relative permeability curves after history matching the CGI process.

Using the aforementioned parameters, the simulation results reproduce the lab experimental results with a very close match. The gas–brine relative permeability curves are consistent with

Table 4. Stone's II Model[58] Parameters for Gas−Water and Water−Oil Relative Permeability in Three-Phase Flow and No Surfactant

gas−water two phase relative permeability							
k_{rwg}^0	k_{rg}^0	S_{wcong}	S_{wcritg}	S_{gcon}	S_{gcrit}	n_{wg}	n_g
0.802	0.874	0.186	0.186	0.000	0.030	1.600	3.700
water−oil two phase relative rermeability							
k_{rwo}^0	k_{ro}^0	S_{wcono}	S_{wcrito}	S_{oirw}	S_{orw}	n_{wo}	n_o
0.802	0.928	0.548	0.550	0.116	0.207	2.584	2.350

the parameters reported in the literature for Estaillades limestone under comparable conditions.[50−52] It is also worth noting that the gas−water relative permeability curve in gas−water two-phase flow does not necessarily have to be the same with that in the three-phase flow. However, we are able to history match (HM) both experimental results using the same set of relative permeability curves in this paper. A reliable three-phase relative permeability curve is very difficult to be obtained, which is still a big challenge in oil and gas industry. The incentive of using the same set of relative permeability data for two-phase flow and three-phase flow in this study is that we do not need to revise the parameter "FMMOB" or the parameters in foam dry-out function when moving from no-oil condition to the condition with oil.

3.1.2. Foam Dry-Out Effect in the Coinjection Process. The high-quality regime foam typically attaches the most interest in EOR because its chemical cost is less compared to that of low-quality foam. The APG surfactant is a good foamer, and its foam strength at the steady state is largely a function of foam quality and injection velocity.[15] Moreover, it is found from the quality scan and velocity scan experiments that several foam states may exist at the steady state, and the MPG is largely a function of foam quality. The discussions of foam behavior in low foam quality are beyond the scope of this paper, and here we focus on high-quality foam experiments.

In these series of experiments, the injection velocity is constant at 4 ft/d while the foam quality varies. The core sample was restored by flushing with 2 wt % NaCl after each test in order to mitigate the foam hysteresis effect.[40] The core sample is regarded as reaching the restored state if the difference in permeability is less than 3% of its original value, which typically requires injection of approximately 30 PV of brine. The combination of foam PG at the steady state for foam quality of 0.5−1.0 is exhibited in Figure 4. The parameters for history matching the steady state foam PG at different foam qualities are listed in Table 5. It can be seen that the simulation results are consistent with the experimental data, as denoted by blue solid line and red asterisk. Different methods[2,10,14] have been proposed to estimate the parameters for foam dry-out effect in the STARS foam model, and the CMOST will provide another approach for rapid procurement of foam modeling parameters.

We are intending to use the same set of simulation parameters to reproduce the foam quality scan data by only adjusting the parameters in foam dry-out function. There are relative large errors for foam quality of 0.8 and 0.9. However, they are already at high foam quality regime, where foam is not stable and may collapse rapidly. Therefore, we may not inject at such high foam quality for EOR. The fractional flow theory was also employed to validate the simulation results. The calculated apparent viscosity (μ_{app}) and gas saturation at the steady state for different foam qualities ($f_g = 0.5−1.0$) match the experimental results reasonably well, as elucidated in Figure 5. The red asterisk and
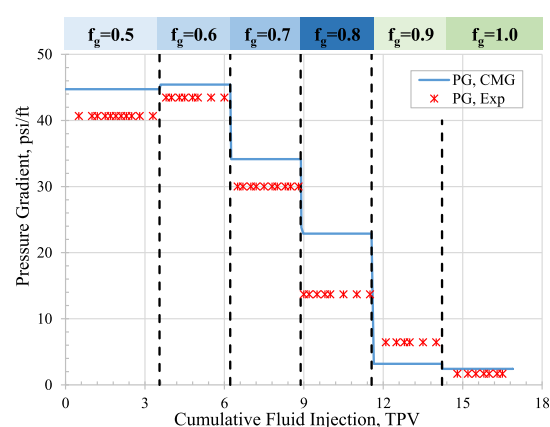

Figure 4. Comparison between the simulation (line) and experimental results (points) of foam PG at different foam qualities, 4 ft/d.

Table 5. Stone's II Model[58] Parameters for Gas−Water and Water−Oil Two-Phase Relative Permeability (with Surfactant)

gas−water two phase relative permeability							
k_{rwg}^0	k_{rg}^0	S_{wcong}	S_{wcritg}	S_{gcon}	S_{gcrit}	n_{wg}	n_g
0.898	0.439	0.044	0.089	0.000	0.141	2.790	2.600
water−oil two phase relative permeability							
k_{rwo}^0	k_{ro}^0	S_{wcono}	S_{wcrito}	S_{oirw}	S_{ow}	n_{wo}	n_o
0.898	0.925	0.295	0.440	0.071	0.090	2.920	1.576

red triangle represent experimental results and simulation results by STARS, respectively, while the red line indicates the predicted results by the fractional flow theory. The equations for calculating foam apparent viscosity during experiments and simulation are listed in eqs 8 and 9.

$$\mu_{app,exp} = \frac{-k_{rock}\nabla P}{u_t} \tag{8}$$

$$\mu_{app,sim} = \frac{1}{k_{rwg}/\mu_w + k_{rg}^f/\mu_g} \tag{9}$$

3.1.3. Critical Capillary Number for Strong Foam Generation. It has been widely acknowledged that there exists a MPG, or correspondingly, a minimum superficial velocity for strong foam to be generated in homogeneous porous media.[19] Estaillades limestone is a relatively heterogeneous core material, but strong foam was also observed at the high flow rate. The foam quality is fixed at 0.6 but the injection rates vary from 1 to 4 ft/d. As shown in Figure 6, there is quite weak foam when the injection rate is 3 ft/d or smaller. However, much stronger foam can be generated at 4 ft/d, and the PG reached the steady state after coinjecting approximately 1.5 TPV fluid. The delay of pressure build up may be largely attributed to the retardation of gas injection by the ISCO pump. After history matching, the parameters for modeling foam generation effect can be obtained, as listed in Table 6.

The existence of multiple steady states during foam displacement has also been reported in the literature.[53] It is capable of interpolating between disparate foam states (RPT and KRINTRP keywords), and several foam states can also be built simultaneously in STARS. As indicated by the green dashed line in Figure 6, a better history matching quality can be
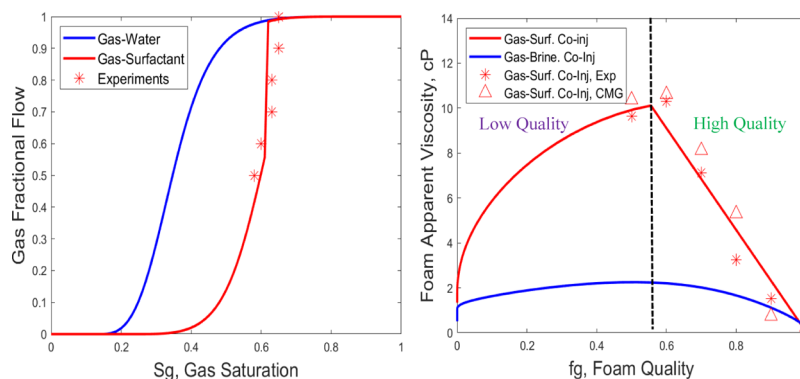
Figure 5. Quality scan experimental data fit to the STARS model, gas saturations in the core sample and foam apparent viscosity are at steady states, co-injection, 4 ft/d.
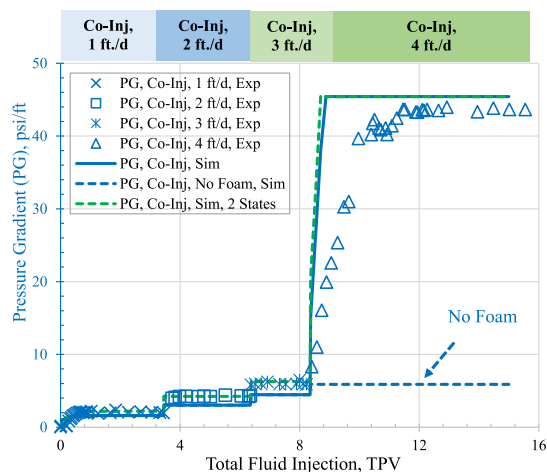

Figure 6. Foam PG as a function of injection rates, 1−4 ft/d, and the foam quality is fixed at 0.6.

obtained after setting different foam strengths and foam states in the foam model.

As a LE model, the capability of STARS foam model to simulate transient foam behavior is still questionable. In the HM process, more data points, for example, PG, were taken from the steady state, and a higher HM weight is set for the data at the steady state. The transient foam behavior may be not well matched compared with that at the steady state. However, the time scale, as shown in Figure 6, is large, and the deviation may be not well identified. Moreover, the APG surfactant is a good

foamer as reported by other researchers. Our hypothesis is that the foam generation may be dominating over foam coalescence during its transport in porous media. This can be proved by the dimensionless time needed to reach the steady state during foam coinjection in the absence of oil. If we subtract the equivalent pore volume (PV) that the ISCO pump compressed itself during foam coinjection, the steady-state foam behavior can be reached after coinjection about 1.0 TPV of liquid and gas.

3.2. Modeling of the Foam EOR Process. The primary objective of this section is to estimate the parameters for the oil destabilization effect on foam to get insights into the foam transport behavior in porous media in the presence of water flooded residual oil and mobile oil. Moreover, foam has been frequently reported as a shear thinning fluid in the literature. The non-Newtonian behavior is also important in simulating foam flow in porous media and will be studied in this section.

3.2.1. Modeling of Oil Flooding and WF. The oil saturation after oil flooding (OF), that is, initial oil saturation, is 0.426 measured by the mass balance. Then, the core sample is aged at reservoir conditions for 48 h. Subsequently, 5.0 PV of synthetic seawater brine was injected into the core, and the water flooded remaining oil saturation is 0.248 (58.2% original oil in place, OOIP). Moreover, water breakthroughs after around 0.07 PV of water injection. Small amount of oil still can be recovered even after 5.0 PV of WF, which may be mainly resulted from oil film drainage and implicates an oil-wet condition of the core sample. The end point relative permeability of oil and water was measured at the end stage of OF and WF, respectively. Based on

Table 6. LE Foam Modeling Parameters in CMG STARS for History Matching the Foam EOR Experiment, as shown in Figure 8

parameters	value	parameters	value
	Foam Modeling without Crude Oil		
DTRAPW	2.371×10^{-2}	KRGCW_foam	1.041×10^{-2}
epgcp	4.900	sfbet	72.444
fmgcp	2.692×10^{-6}	SFDRY (without oil)	0.383
FMMOB	42.170	SGR	0.252
surface tension	27.000 mN/m	surfactant MW	430 g/mol
	Foam Modeling with Crude Oil		
ADMAXT	3.648×10^{-6} gmol/cm^3	epsurf	1.590
ADSLANG1	3.981 gmol/cm^3	floil	0.084
ADSLANG2	1.148×10^{5}	fmcap	1.218×10^{-5}
DISPI_WAT	0.092 cm^2/min	fmoil	0.249
epoil	1.038	fmsurf	4.624×10^{-6}
epcap	1.600	SFDRY (with oil)	0.305

the performance of WF, we may conclude that the core sample is close to oil wet.

The oil injection rates are 8, 0.5, and 0.2 ft/d during OF, whereas the water injection rate is 4 ft/d during WF. The PG, effluent oil fraction, and cumulative oil recovery during water injection are recorded during experiments. CMOST is applied to assist history matching the PG, cumulative oil production (COP), and cumulative water production (CWP) during OF and WF process. The comparison between experimental and simulation results is exhibited in Figure 7.
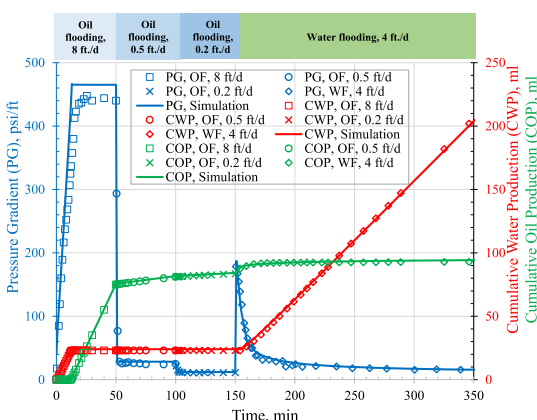
Figure 7. PG, CWP, and COP during OF (8, 0.5, and 0.2 ft/d) and WF (4 ft/d).

The OF and WF experiments were reproduced by just tuning water−oil two-phase relative permeability curves in the 1D reservoir model. The water−oil two-phase relative permeability curves are assumed to follow Corey's correlation,[49] as listed in the Supporting Information (S3). The water−oil two-phase relative permeability curve obtained from unsteady tests, that is, OF and WF, is consistent with that reported in the literature.[50,54,55] The input values for simulating OF and WF are listed in Table 4.

3.2.2. Modeling Foam Transport in the Presence of Water-Flooded Residual Oil. At the end stage of WF, the in situ salinity inside the core sample is hypothesized to be close to the injection salinity, therefore, the effect of salinity on foam is neglected in the simulation. After WF, a 0.40 PV slug of surfactant was injected (4 ft/d) prior to foam coinjection in order to compensate for surfactant retention. It is found that the PG across the core sample decreases with continuous injection of surfactant solution, which may indicate that the surfactant (or IFT) has noticeable effect on the water−oil relative permeability.[56,57] This hypothesis is supported by IFT measurement at 131 F, in which the oil-brine IFT decreased from 34.5 (±0.7) mN/m to 0.29 (±0.1) mN/m after adding 0.2 wt % APG surfactant. Thus, the relative permeability curve in the presence of surfactant needs to be modified, as indicated in Table 5.

As for foam flooding, the foam quality is fixed at 0.6 while the total injection rate varies from 4 to 20 ft/d. The concentration of APG surfactant in effluents was accurately analyzed by the HPLC method. It is found that the surfactant breakthroughs after coinjecting around 4.2 TPV of surfactant solution and nitrogen, which is equivalent to 2.0 liquid PV including surfactant preflush. Therefore, the surfactant retention/adsorption is crucial and also needs to be considered in the foam model. Foam was observed from the outlet after surfactant breakthrough. Clear foam was found at 8 ft/d when oil

saturation decreased to 14% OOIP ($S_o = 0.067$). Shear thinning foam behavior was observed when the injection velocity is higher than 12 ft/d (PG is around 120 psi/ft). Therefore, the parameters for modeling the foam shearing thinning behavior also need to be incorporated into the model.

For history matching foam process with crude oil, the parameters for surfactant effect, oil effect, and shear thinning effect are further included into the foam model, where the parameters for foam dry-out and foam generation remain identical to those in the absence of crude oil. The surfactant retention/adsorption and dispersion are also important and were studied in the model. However, the surfactant partition between oil and water is not considered in this study. One may get this information by static bottle tests or dynamic core flooding tests (with crude oil). Stone's II model was assumed for the three-phase relative permeability curve correlation.[58] Figure 8 shows the comparison of the PG, cumulative oil recovery
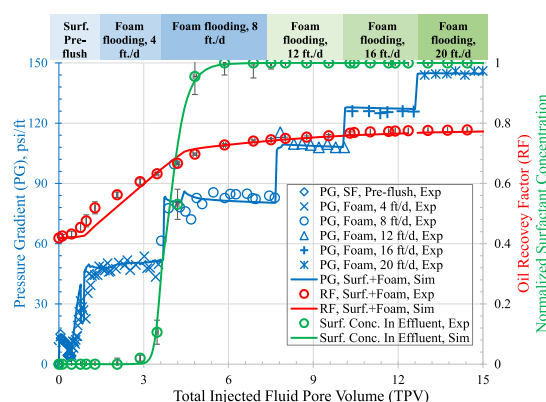

Figure 8. Comparison between simulation and experimental results of the PG, cumulative oil recovery, and normalized surfactant concentration during foam flooding, 4−20 ft/d.

factor, and normalized effluent surfactant concentration between simulation results and the experimental results after history matching.

It can be seen that the foam EOR process can be reasonably reproduced using the parameters, as listed in Table 6. The simulation data set is found in the Supporting Information (S4). Around 30% OOIP was recovered after injection about 4.90 TPV of surfactant and nitrogen. However, there is some error in reading the volume of oil in the effluents. Ultraviolet (UV) or infrared radiation could be employed to accurately quantify the amount of oil in the effluents. The oil recovery rate is quite slow because of (i) foam collapse at the displacement front and (ii) surfactant retention/adsorption. It is also worth noting that the gas is injected from the bottom of core sample, which is not a favorable displacement and may cause early gas breakthrough. If gas is injected from the top, the foam EOR process may be even more effective.

The profiles of oil saturation, water saturation, gas saturation, pressure, surfactant adsorption, and gas mobility at $t = 200$ min (TPV = 3.3) are shown in Figure 9. We can see from the simulation results that foam can be readily generated but it will collapse at the displacement front because of the high oil saturation, therefore, the oil bank moves very slowly, and the oil cut is small.

Moreover, it is found from simulation results that the surfactant adsorption is severe. In this case, the surfactant will first be adsorbed on the mineral, and foam may only be
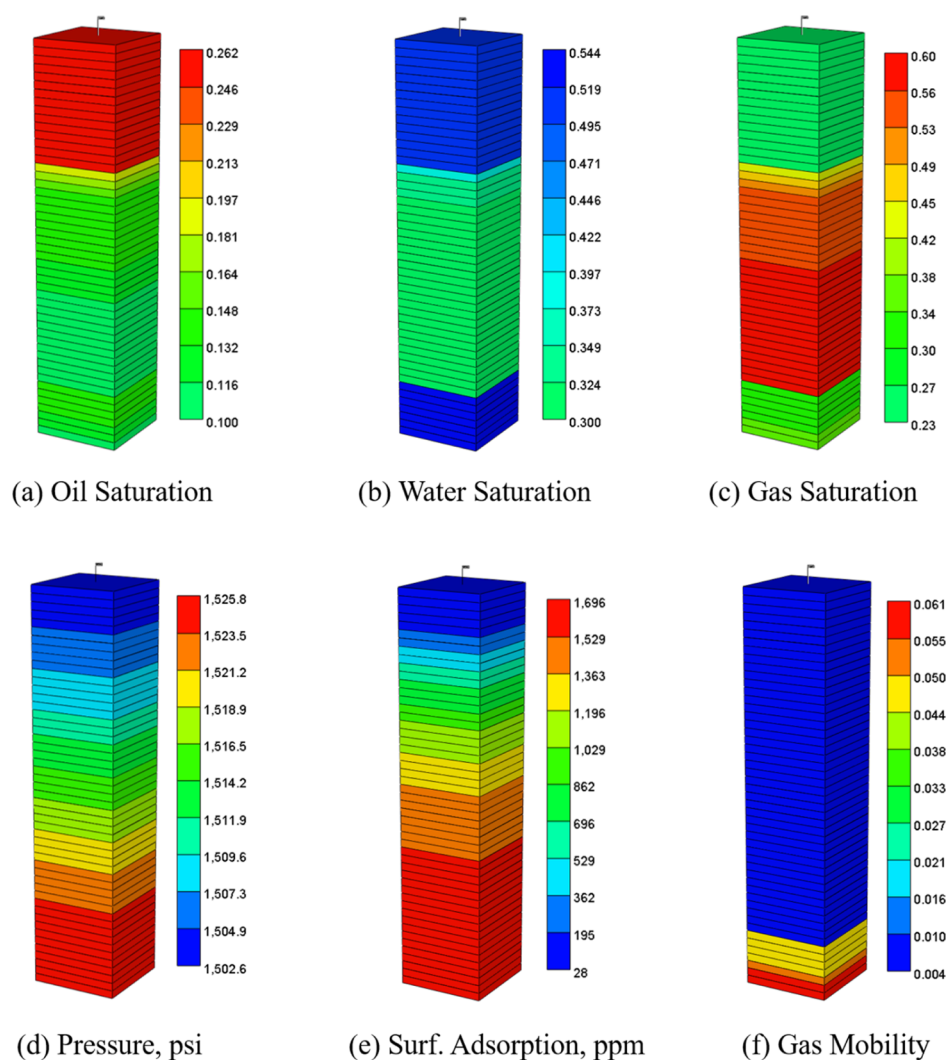
Figure 9. Profiles of (a) oil saturation, (b) water saturation, (c) gas saturation, (d) pressure (in psi), (e) surfactant adsorption (in ppm), and (f) gas mobility at t = 200 min during foam flooding (total injection PV = 3.3 TPV).
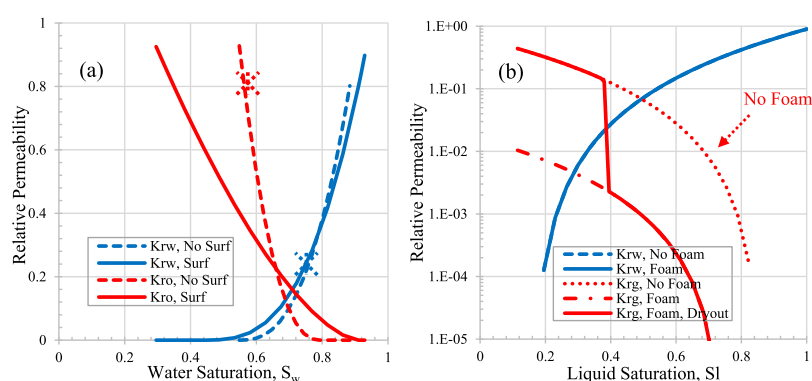

Figure 10. (a) Water−oil two-phase relative permeability curves in the presence and absence of surfactant; and (b) gas−water relative permeability curves in the presence and absence of foam.

generated at places where the requirement of adsorption has been locally satisfied during continuous surfactant injection. This may be also the primary reason why the foam front moves so slowly, and this issue may become even worse when a limited slug of surfactant is proposed. In order to decrease surfactant adsorption/retention, alkali or sacrificial agent can be used.[59]

The water−oil relative permeability in the presence and absence of surfactant is illustrated in Figure 10a. As indicated before, surfactant has notable effects on water−oil two-phase relative permeability. Figure 10b illustrates the effect of foam on gas relative permeability. In the STARS LE foam model, only the gas relative permeability is modified with the help of foam while

the water relative permeability and gas viscosity are regarded as unaffected.

3.2.3. Modeling Foam Transport in the Presence of Mobile Oil. The oil fractional flow tests were conducted after foam coinjection. Based on the Buckley–Leverett theory,[60] the oil saturation could be increased by increasing the flow fraction of oil. This test can be used to investigate the effect of oil saturation on foam strength.[46] It should be noted that emulsion could also be formed during oil fractional tests, which add complexity into modeling of oil fractional flow tests.

Figure 11 shows the comparison of the simulated PG with experimental observations using the parameters, as shown in
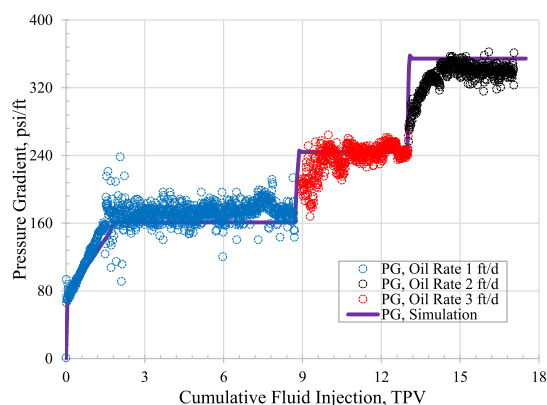
Figure 11. PG at different oil flow rates (1, 2, and 3 ft/d) during foam/oil fractional flow tests (total velocity of surfactant solution and gas is fixed at 4 ft/d).

Tables 5 and 6, during foam/oil fractional flow tests. The total flow rate of gas and surfactant solution is fixed at 4 ft/d while the oil flow rate varies from 1 to 3 ft/d. Moreover, the foam quality is 0.6 in the oil fractional flow tests. An insight into the simulation results revels that there is almost no foam when the oil fractional flow is 10% or higher because the oil saturation is higher than fmoil.

3.3. DISCUSSION

3.3.1. Influence of Foam Quality on EOR. The calculated cumulative oil recovery for foam coinjection at 4 ft/d with different foam qualities is elucidated in Figure 12, using the same set of simulation parameters, as shown in Table 5. The initial oil saturation when foam flooding starts is 41.90% OOIP (S_o =
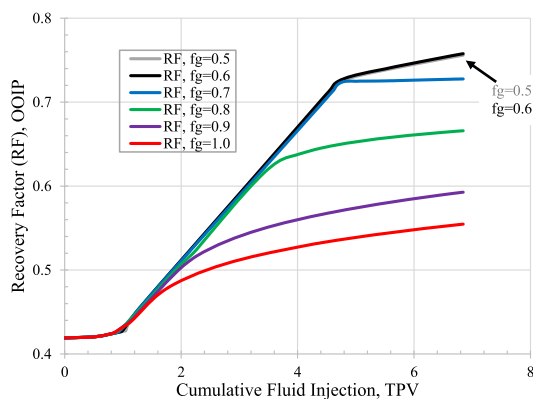
Figure 12. Effect of foam quality on improved oil recovery (total superficial velocity of surfactant solution and gas is fixed at 4 ft/d).

0.247). Before foam coinjection, a 0.50 PV slug of surfactant was injected. We can see that there is no appreciable difference in oil recovery between 50 and 60% foam quality. Considering the cost for surfactant, injection foam at 60% foam quality performs better than that with 50% foam quality. When the foam quality increases from 60 to 100%, the cumulative oil recovery after 7 TPV coinjection decreases from 75.8 to 55.5% OOIP. This is probably because the (i) surfactant transport is slower at high foam quality because of surfactant retention; and (ii) foam strength is smaller when foam quality is larger than 60%.

3.3.2. Effect of Oil on Foam Strength. The effect of crude oil on foam simulation has been extensively simulated using the fractional flow theory,[47,61−63] PB foam model,[64] and LE foam model.[33,46] In this section, the effect of oil on foam strength is evaluated by a simplified STARS foam model. Figure 13 summarizes the effect of oil on steady-state foam PG by a so-called wet-foam model.[66,67] Only the foam mobility reduction factor (FM) is modified in the calculation, as described in eqs 10 and 11.

The parameters for F_{dry} and F_{oil} functions are the same as those shown in Table 4. As shown in Figure 13, the presence of oil has detrimental effect on the PG but negligible effect on the transition foam quality. When the oil saturation increases from 0 to 0.2, the foam stability decreases evidently.

$$\mathrm{FM} = \frac{1}{1 + \mathrm{FMMOB} \times F_{dry} \times F_{oil}} \qquad (10)$$

$$\nabla p = \mu_g \frac{u_g}{k_{rock} k_{rg}^f} \qquad (11)$$

3.3.3. Sensitivity Analysis of Foam Modeling Parameters. Sensitivity analysis can be applied to find out the dominating factor in designing a successful foam EOR process. It has been reported that the water- and gas-relative permeability, in particular, the water-relative permeability exponent, and connate water saturation are important.[65] Surfactant adsorption and foam quality are also of great importance. However, we are only performing sensitivity analysis for parameters of F_1, F_2, F_3, F_4, and F_{dry} functions in the LE foam model in this study. The ranges of different parameters studied for sensitivity analysis are illustrated in Table 7.

A comprehensive evaluation reveals that the foam EOR process is most sensitive to limiting water saturation (SFDRY) and oil destabilization effect (fmoil), as illustrated in the tornado plot in Figure 14. More specifically, the PG at the steady state is largely influenced by parameter SFDRY, followed by FMCAP, FMMOB, FMOIL, FMGCP, and SFBET, in the decreasing order. Comparatively, the calculated oil recovery factor is greatly dominated by FMOIL, FMCAP, and EPOIL but relatively less sensitive to FMMOB, SFDRY, and EPCAP. It is also worth noting that the sensitivity analysis is largely dependent on the ranges of parameters investigated, and these conclusions may not be applied universally. Moreover, the foam shear thinning effect and maximum foam strength are also crucial in accurate modeling of foam EOR process.

It is also important to discuss the effect of initial guess and solution uniqueness in this section. In this process, the designed exploration and controlled evolution (DECE) algorithm is used, and the optimized objective solution or HM quality is insensitive to the initial guess. DECE optimization is an iterative process that first applies a designed exploration stage and then a controlled evolution stage. In the designed exploration process,
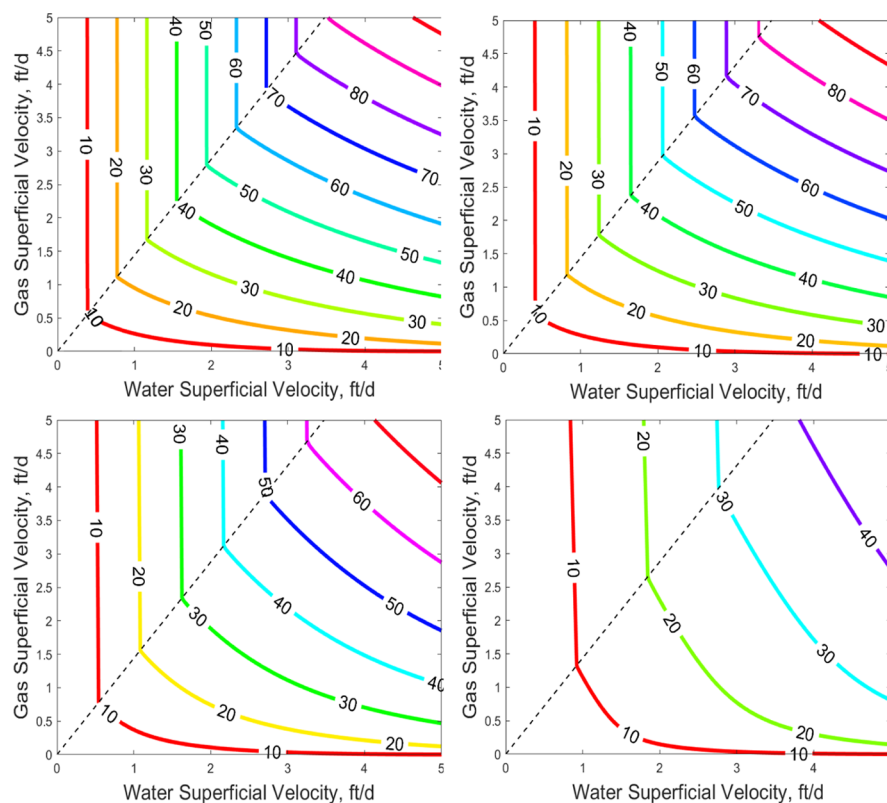
Figure 13. Contour plot of PG (psi/ft) as a function of water and gas superficial velocities predicted by the wet-foam model at fixed oil saturation $S_o = 0$ (top left), $S_o = 0.1$ (top right), $S_o = 0.15$ (bottom left), and $S_o = 0.2$ (bottom right).

Table 7. Ranges of STARS LE Foam Model Parameters for Sensitivity Analysis

parameters	ranges	parameters	ranges	parameters	ranges
epcap	0.5−5.0	fmcap	$1 \times 10^{-5.5}$ to 1×10^{-4}	sfbet	100−100,000
epgcp	0.5−6.5	fmgcp	$1 \times 10^{-6.5}$ to $1 \times 10^{-5}.5$	SFDRY	0.20−0.40
epoil	0.5−5.0	FMMOB	10−1000	SGR	0.10−0.35
epsurf	0.5−5.0	fmoil	0.15−0.35		
floil	0−0.15	fmsurf	1×10^{-6} to 1×10^{-4}		

the objective is to evaluate the search space in a designed random manner such that maximum information can be obtained from representative simulation datasets. Based on this initial analysis, the DECE algorithm scrutinizes every candidate value of each parameter to determine a better chance to improve the HM quality. In the controlled evolution stage, statistical analyses are performed for the simulation results obtained in the designed exploration stage. Among the physical range of candidate parameters, the unique physical solution was found after HM.

Furthermore, the combined use of F_{dry} and F_4 function would require at least one foam quality scan and one velocity scan experiments. Additionally, researchers have found in the past that the velocity scan in the low-quality regime is more sensitive than that in the high-quality regime and concluded that foam is shear-thinning in the low-quality regime and almost Newtonian in the high-quality regime. Selecting these points is important in determining the sensitivity of the foam model parameters and to avoid multiple sets of parameters that appear to work equivalently well in some cases.

4. CONCLUSIONS

In this paper, we present an integrated workflow to obtain the parameters in the LE foam model by history matching a series of reliable laboratory experiments performed at reservoir conditions on Estaillades limestone using a commercial reservoir simulator. Moreover, sensitivity analysis of foam modeling parameters is investigated to determine the most dominating parameters for accurate simulation of foam EOR process in porous media. The main conclusions are summarized in the following:

1. Around 30% OOIP was recovered in the laboratory after injecting about 4.90 TPV of surfactant and nitrogen (60% foam quality) at reservoir condition, demonstrating large potential for EOR on carbonate by foam;

2. An integrated workflow is demonstrated to obtain the physical parameters for the LE foam model by history matching a series of laboratory experiments using CMG STARS and CMOST;

3. The calculated results reproduce the WF and foam flooding experimental outputs reasonably well. The oil saturation function (F_2) and foam dry-out function (F_{dry}) are important in accurate modeling of foam EOR process;
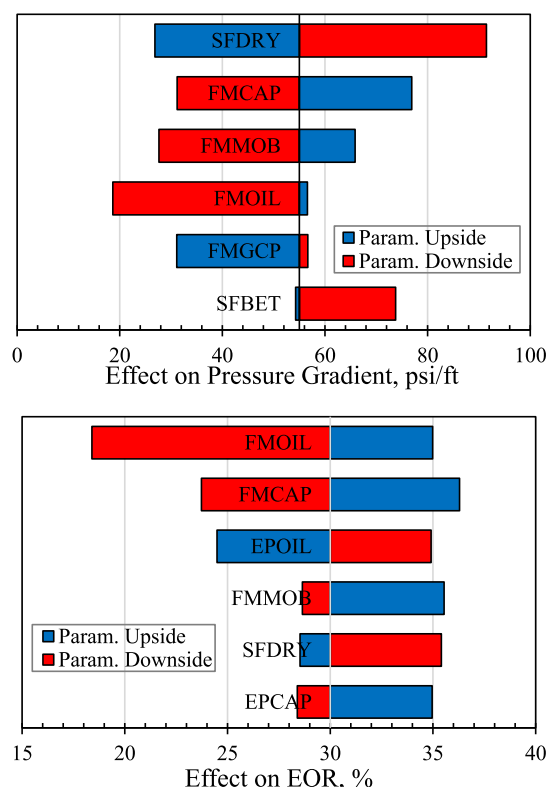
Figure 14. Sensitivity of parameters in F_1, F_2, F_3, F_4, and F_{dry} in the LE foam model.

4 CMG STARS and CMOST can be of great help in estimating the foam modeling parameters and interpreting the complex lab foam flooding results.

ASSOCIATED CONTENT

Supporting Information

The Supporting Information is available free of charge at https://pubs.acs.org/doi/10.1021/acsomega.0c03401.

Description of the experimental procedures, different functions in the STARS LE foam model, Stone's II model for three-phase relative permeability correlation, and example data file for CMG STARS (PDF)

AUTHOR INFORMATION

Corresponding Authors

Lei Ding — Department of Petroleum Engineering, Texas A&M University at Qatar, Doha 23874, Qatar; orcid.org/0000-0001-8648-8657; Email: lei.ding@qatar.tamu.edu

Leyu Cui — Total S. A., E&P, Lacq 64170, France; orcid.org/0000-0003-2164-7586; Email: leyu.cui@total.com

Dominique Guérillot — Department of Petroleum Engineering, Texas A&M University at Qatar, Doha 23874, Qatar; Email: dominique.guerillot@qatar.tamu.edu

Authors

Stephane Jouenne — Total S. A., E&P, Lacq 64170, France
Oussama Gharbi — Total S. A., E&P, Lacq 64170, France
Mayur Pal — North Oil Company, Doha 21264, Qatar
Henri Bertin — I2M, CNRS, University of Bordeaux, Bordeaux INP, Talence 33400, France

Mohammad Azizur Rahman — Department of Petroleum Engineering, Texas A&M University at Qatar, Doha 23874, Qatar

Carolina Romero — Total S. A., E&P, Lacq 64170, France

Complete contact information is available at:
https://pubs.acs.org/10.1021/acsomega.0c03401

Notes

The authors declare no competing financial interest.

ACKNOWLEDGMENTS

NOMENCLATURE

C_s, surfactant concentration, mol/L

DTRAPW, a value of interpolation parameter for rock-fluid data set in CMG

FM, dimensionless interpolation factor for gas relative permeability reduction

F_1, interpolation factor for surfactant function

F_2, interpolation factor for oil saturation function

F_3, interpolation factor for capillary number on foam strength

F_4, interpolation factor for capillary number on foam generation

F_{dry}, interpolation factor for foam dry-out function

f_g, foam quality, or gas fractional flow

FMMOB, maximum interpolation factor for gas relative permeability reduction

fmsurf, critical surfactant concentration in F_1, mol/L

epsurf, exponent for surfactant concentration in F_1

floil, critical surfactant concentration in F_1

fmoil, critical oil saturation in F_2

fmgcp, critical capillary number for strong foam generation in F_4

fmcap, critical capillary number for foam non-Newtonian behavior in F_3

epgcp, exponent for strong foam generation in F_4

epcap, exponent for foam non-Newtonian behavior in F_3

KRINTRP, an interpolation set number in CMG

N_{ca}, capillary number

SFDRY, limiting water saturation in F_{dry}

sfbet, parameter regulating the slope of F_{dry} near SFDRY

k_{rock}, permeability of rock, mD

k_{rj}, relative permeability of phase j

k_{rwo}, relative permeability of water in water−oil two phase flow

k_{rwo}^0, end point relative permeability of water in water−oil two phase flow

k_{ro}^0, end point relative permeability of oil

k_{row}, relative permeability of oil

k_{rg}^0, end point relative permeability of gas

k_{rg}^f, relative permeability of gas, with foam

k_{rg}^{nf}, relative permeability of gas, no foam

k_{rwg}, relative permeability of water in gas water two phase flow

k_{rwg}^0, end point water relative permeability in gas water two phase flow

S_{wcong}, connate water saturation in gas water two phase flow

S_{wcritg}, critical water saturation by gas flooding

S_{gcon}, connate gas saturation

S_{gcrit}, critical gas saturation

n_{wg}, corey exponents for water in gas water two phase flow

∇p, pressure gradient, psi/ft

SFDRY, limiting water saturation in foam dry-out function

SFBET, a parameter controlling the abruptness of foam coalescence near SFDRY

SGR, residual gas saturation

S_j, saturation of phase j

S_{wcrito}, critical water saturation by OF

S_{oirw}, irreducible oil saturation by water flooding

n_{wo}, corey exponents for water in water−oil two phase flow

S_{wcono}, connate water saturation in water−oil two phase flow

S_{orw}, critical oil saturation by water flooding

n_{g}, corey exponents for gas

n_{o}, corey exponents for oil

S_{wc}, connate water saturation

S_{gr}, residual gas saturation

$\bar{u}_j$, superficial velocity of phase j, ft/d

μ_{app}, apparent viscosity of foam, cP

μ_j, dynamic viscosity of phase j, cP

■ SUBSCRIPTS

j the j phase, oil water or gas

g   the gas phase

o   the oil phase

t   the total phases

w   the water phase

■ SUPERSCRIPTS

f   with foam

nf   without foam

0   end point relative permeability

■ REFERENCES

(1) Blaker, T.; Celius, H. K.; Lie, T.; Martinsen, H. A.; Rasmussen, L.; Vassenden, F. Foam for gas mobility control in the Snorre field: the FAWAG project. *Annual Technical Conference and Exhibition*; SPE, 1999.

(2) Ma, K.; Lopez-Salinas, J. L.; Puerto, M. C.; Miller, C. A.; Biswal, S. L.; Hirasaki, G. J. Estimation of parameters for the simulation of foam flow through porous media. Part 1: the dry-out effect. *Energy Fuels* 2013, 27, 2363−2375.

(3) Andrianov, A.; Farajzadeh, R.; Mahmoodi Nick, M.; Talanana, M.; Zitha, P. L. J. Immiscible foam for enhancing oil recovery: bulk and porous media experiments. *Ind. Eng. Chem. Res.* 2012, 51, 2214−2226.

(4) Kovscek, A. R.; Radke, C. J. *Fundamentals of Foam Transport in Porous Media*, 1994.

(5) Shah, S. Y.; Wolf, K.-H.; Pilus, R. M.; Rossen, W. R. Foam Generation by Capillary Snap-Off in Flow Across a Sharp Permeability Transition. *Soc. Pet. Eng. J.* 2019, 24, 116−128.

(6) Dicksen, T.; Hirasaki, G. J.; Miller, C. A. Conditions for foam generation in homogeneous porous media. *SPE/DOE Symposium Improved Oil Recovery*, 2002.

(7) Gauglitz, P. A.; Friedmann, F.; Kam, S. I.; Rossen, W. R. Foam generation in homogeneous porous media. *Chem. Eng. Sci.* 2002, 57, 4037−4052.

(8) Rossen, W. R. Theory of mobilization pressure-gradient of flowing foams in porous media.1. Incompressible foam. *J. Colloid Interface Sci.* 1990, 136, 1−16.

(9) Dicksen, T.; Hirasaki, G. J.; Miller, C. A. Mobility of foam in heterogeneous media: Flow parallel and perpendicular to stratification. *Annual Technical Conference and Exhibition*; SPE, 2002; Vol. 7, p 203.

(10) Zeng, Y.; Muthuswamy, A.; Ma, K.; Wang, L.; Farajzadeh, R.; Puerto, M.; Vincent-Bonnieu, S.; Eftekhari, A. A.; Wang, Y.; Da, C.; Joyce, J. C.; Biswal, S. L.; Hirasaki, G. J. Insights on foam transport from a texture-implicit local-equilibrium model with an improved parameter estimation algorithm. *Ind. Eng. Chem. Res.* 2016, 55, 7819−7829.

(11) Falls, A. H.; Hirasaki, G. J.; Patzek, T. W.; Gauglitz, D. A.; Miller, D. D.; Ratulowski, T. Development of a mechanistic foam simulator: the population balance and generation by snap-off. *SPE Reservoir Eng.* 1988, 3, 884−892.

(12) Ransohoff, T. C.; Radke, C. J. Mechanisms of foam generation in glass bead packs. *SPE Reservoir Eng.* 1988, 3, 573−585.

(13) Alvarez, J. M.; Rivas, H. J.; Rossen, W. R. Unified model for steady-state foam behavior at high and low foam qualities. *Soc. Pet. Eng. J.* 2001, 6, 325−333.

(14) Boeije, C. S.; Rossen, W. Fitting foam-simulation-model parameters to data: I. coinjection of gas and liquid. *SPE Reservoir Eval. Eng.* 2015, 18, 264−272.

(15) Boeije, C. S.; Rossen, W. R. SAG foam flooding in carbonate rocks. *J. Pet. Sci. Technol.* 2018, 171, 843−853.

(16) Farajzadeh, R.; Lotfollahi, M.; Eftekhari, A. A.; Rossen, W. R.; Hirasaki, G. J. H. Effect of permeability on implicit-texture foam model parameters and the limiting capillary pressure. *Energy Fuels* 2015, 29, 3011−3018.

(17) Khatib, Z. I.; Hirasaki, G. J.; Falls, A. H. Effects of capillary pressure on coalescence and phase mobilities in foams flowing through porous media. *SPE Reservoir Eng.* 1988, 3, 919−926.

(18) Rossen, W. R.; van Duijn, C. J.; Nguyen, Q. P.; Shen, C.; Vikingstad, A. K. Injection strategies to overcome gravity segregation in simultaneous gas and water injection into homogeneous reservoirs. *Soc. Pet. Eng. J.* 2010, 15, 76−90.

(19) Yu, G.; Rossen, W. R.; Vincent-Bonnieu, S. Coreflood Study of Effect of Surfactant Concentration on Foam Generation in Porous Media. *Ind. Eng. Chem. Res.* 2019, 58, 420−427.

(20) Hirasaki, G. J.; Lawson, J. B. Mechanisms of foam flow in porous media: apparent viscosity in smooth capillaries. *Soc. Pet. Eng. J.* 1985, 25, 176−190.

(21) Bernard, G. G.; Jacobs, W. L. Effect of foam on trapped gas saturation and on permeability of porous media to water. *Soc. Pet. Eng. J.* 1965, 5, 295−300.

(22) Eftekhari, A. A.; Farajzadeh, R. Effect of foam on liquid phase mobility in porous media. *Sci. Rep.* 2017, 7, 43870.

(23) Ma, K.; Ren, G.; Mateen, K.; Morel, D.; Cordelier, P. Modeling techniques for foam flow in porous media. *Soc. Pet. Eng. J.* 2015, 20, 453−470.

(24) Kovscek, A. R.; Chen, Q.; Gerritsen, M. Modeling foam displacement with the local-equilibrium approximation: theory and experimental verification. *Soc. Pet. Eng. J.* 2010, 15, 171−183.

(25) Ma, K.; Mateen, K.; Ren, G.; Luo, H.; Bourdarot, G.; Morel, D. Mechanistic Modeling of Foam Flow Through Porous Media in the Presence of Oil: Review of Foam-Oil Interactions and an Improved Bubble Population-Balance Model. *Annual Technical Conference and Exhibition*; SPE, 2018.

(26) Kovscek, A. R.; Patzek, T. W.; Radke, C. J. A mechanistic population balance model for transient and steady-state foam flow in Boise sandstone. *Chem. Eng. Sci.* 1995, 50, 3783−3799.

(27) Bertin, H. J.; Apaydin, O. G.; Castanier, L. M.; Kovscek, A. R. Foam flow in heterogeneous porous media: Effect of crossflow. *SPE/DOE Symposiyum Improved Oil Recovery*, 1998.

(28) Gassara, O.; Douarche, F.; Braconnier, B.; Bourbiaux, B. Equivalence between semi-empirical and population-balance foam models. *Transp. Porous Media* 2017, 120, 473−493.

(29) Lotfollahi, M.; Farajzadeh, R.; Delshad, M.; Varavei, A.; Rossen, W. R. Comparison of implicit-texture and population-balance foam models. *J. Nat. Gas Sci. Eng.* 2016, 31, 184−197.

(30) Lotfollahi, M.; Kim, I.; Beygi, M. R.; Worthen, A. J.; Huh, C.; Johnston, K. P.; Wheeler, M. F.; DiCarlo, D. A. Foam generation hysteresis in porous media: Experiments and new insights. *Transp. Porous Media* 2017, 116, 687−703.

(31) Spirov, P.; Rudyk, S. Testing of Snorre field foam assisted water alternating gas (FAWAG) performance in new foam screening model. *Oil Gas Sci. Technol.* **2015**, *70*, 1025−1033.

(32) Aydin, E. Numerical simulation and history matching of steam-foam process to enhance heavy oil recovery. Ph.D Dissertation, The University of Texas at Austin, 2019.

(33) Hosseini-Nasab, S. M.; Douarche, F.; Simjoo, M.; Nabzar, L.; Bourbiaux, B.; Zitha, P. L. J.; Roggero, F. Numerical simulation of foam flooding in porous media in the absence and presence of oleic phase. *Fuel* **2018**, *225*, 655−662.

(34) Zeng, Y.; Farajzadeh, R; Biswal, S. L.; Hirasaki, G. J. A 2-D simulation study on CO_2 soluble surfactant for foam enhanced oil recovery. *J. Ind. Eng. Chem.* **2019**, *72*, 133−143.

(35) Zeng, Y.; Kamarul Bahrim, R. Z.; Groot, J. A. W. M.; Vincent Bonnieu, S.; Groenenboom, J.; Mohd Shafian, S. R.; Abdul Manap, A. A.; Tewari, R. D.; Mohammadian, E.; Azdarpor, A.; Hamidi, H. Probing Methane Foam Transport in Heterogeneous Porous Media: An Experimental and Numerical Case Study of Permeability-Dependent Rheology and Fluid Diversion at Field Scale. *Soc. Pet. Eng. J.* **2020**, *25*, 1697.

(36) *CMG User's Guide STARS Advanced Process and Thermal Reservoir Simulator*, 2017.10; Computer Modeling Group.

(37) Farajzadeh, R.; Andrianov, A.; Krastev, R.; Hirasaki, G. J.; Rossen, W. R. Foam−oil interaction in porous media: implications for foam assisted enhanced oil recovery. *Adv. Colloid Interface Sci.* **2012**, *183−184*, 1−13.

(38) AlMaqbali, A.; Agada, S.; Geiger, S.; Haugen, Å.; Fernø, M. A. Modelling foam displacement in fractured carbonate reservoirs. *Abu Dhabi International Petroleum Exhibition and Conference*, 2015.

(39) Ren, G.; Yu, W. Numerical investigations of key aspects influencing CO_2 foam performance in fractured carbonate system using CO_2 soluble surfactants. *J. CO_2 Util.* **2019**, *33*, 96−113.

(40) Kahrobaei, S.; Vincent-Bonnieu, S.; Farajzadeh, R. Experimental study of hysteresis behavior of foam generation in porous media. *Sci. Rep.* **2017**, *7*, 8986.

(41) Kahrobaei, S.; Farajzadeh, R. Insights into Effects of Surfactant Concentration on Foam Behavior in Porous Media. *Energy Fuels* **2019**, *33*, 822−829.

(42) Abbaszadeh, M.; Varavei, A.; Rodriguez-de la Garza, F.; Villavicencio, A. E.; Lopez Salinas, J.; Puerto, M. C.; Hirasaki, G.; Miller, C. A. Methodology for the Development of Laboratory-Based Comprehensive Foam Model for Use in the Reservoir Simulation of Enhanced Oil Recovery. *Soc. Pet. Eng. J.* **2018**, *21*, 344−363.

(43) Kapetas, L.; Vincent-Bonnieu, S.; Farajzadeh, R.; Eftekhari, A. A.; Mohd-Shafian, S. R.; Bahrim, R. K.; Rossen, W. Effect of permeability on foam-model parameters-an integrated approach from coreflood experiments through to foam diversion calculations. *IOR 2015−18th European Symposium on Improved Oil Recovery*, 2015.

(44) Kapetas, L.; Bonnieu, S.; Danelis, S.; Rossen, W. R.; Farajzadeh, R.; Eftekhari, A. A.; Mohd Shafian, S. R.; Bahrim, R. Z. K. Effect of temperature on foam flow in porous media. *J. Ind. Eng. Chem.* **2016**, *36*, 229−237.

(45) Cui, L.; Ma, K.; Puerto, M.; Abdala, A. A.; Tanakov, I.; Lu, L. J.; Chen, Y.; Elhag, A.; Johnston, K. P.; Biswal, S. L.; Hirasaki, G. Mobility of ethomeen C12 and carbon dioxide (CO2) foam at high temperature/high salinity and in carbonate cores. *Soc. Pet. Eng. J.* **2016**, *21*, 1151−1163.

(46) Jian, G.; Zhang, L.; Da, C.; Puerto, M.; Johnston, K. P.; Biswal, S. L.; Hirasaki, G. J. Evaluating the Transport Behavior of CO2 Foam in the Presence of Crude Oil under High-Temperature and High-Salinity Conditions for Carbonate Reservoirs. *Energy Fuels* **2019**, *33*, 6038−6047.

(47) Tang, J.; Castañeda, P.; Marchesin, D.; Rossen, W. R. Three-Phase Fractional-Flow Theory of Foam-Oil Displacement in Porous Media with Multiple Steady States. *Water Resour. Res.* **2019**, *55*, 10319−10339.

(48) Huh, D. G.; Handy, L. L. Comparison of steady and unsteady-state flow of gas and foaming solution in porous media. *SPE Reservoir Eng.* **1989**, *4*, 77−84.

(49) Corey, A. T. The Interrelation Between Gas and Oil Relative Permeabilities. *Prod. Mon.* **1954**, *19*, 38−41.

(50) Ott, H.; Pentland, C. H.; Oedai, S. CO2−brine displacement in heterogeneous carbonates. *Int. J. Greenhouse Gas Control* **2015**, *33*, 135−144.

(51) Suicmez, V. S.; Piri, M.; Blunt, M. J. Pore-scale simulation of water alternate gas injection. *Transp. Porous Media* **2007**, *66*, 259−286.

(52) Egermann, P.; Vizika, O.; Dallet, L.; Requin, C.; Sonier, F. Hysteresis in three-phase flow: experiments, modeling and reservoir simulations. *SPE European Petroleum Conference*; SPE, 2000.

(53) Rossen, W. R.; Bruining, J. Foam Displacements with Multiple Steady States. *J. Pet. Sci. Eng.* **2007**, *12*, 5−18.

(54) Blunt, M. J.; Bijeljic, B.; Dong, H.; Gharbi, O.; Iglauer, S.; Mostaghimi, P.; Paluszny, A.; Pentland, C. Pore-scale imaging and modelling. *Adv. Water Resour.* **2013**, *51*, 197−216.

(55) Nono, F.; Bertin, H.; Hamon, G. Oil recovery in the transition zone of carbonate reservoirs with wettability change: hysteresis models of relative permeability versus experimental data. *Proceedings of Society of Core Analysts Held in Avignon, France, SCA2014-007*, 2014.

(56) Lake, L. W.; Johns, R.; Rossen, W.; Pope, G. A. *Fundamentals of Enhanced Oil Recovery*; SPE: Richardson, 2014.

(57) Jahanbakhsh, A.; Shahverdi, H.; Sohrabi, M. Gas/oil relative permeability normalization: effects of permeability, wettability, and interfacial tension. *SPE Reservoir Eval. Eng.* **2016**, *19*, 673−682.

(58) Stone, H. L. Estimation of three-phase relative permeability and residual oil data. *J. Can. Pet. Technol.* **1973**, *12*, 53−61.

(59) Hirasaki, G.; Miller, C. A.; Puerto, M. Recent Advances in Surfactant EOR. *SPE J.* **2011**, *16*, 889−907.

(60) Buckley, S. E.; Leverett, M. C. Mechanism of fluid displacement in sands. *Trans. Am. Inst. Min., Metall. Pet. Eng.* **1942**, *146*, 107−116.

(61) Ashoori, E.; van der Heijden, T.; Rossen, W. Fractional-flow theory of foam displacements with oil. *SPE J.* **2010**, *15*, 260−273.

(62) Kam, S. I.; Nguyen, Q. P.; Li, Q.; Rossen, W. R. Dynamic simulations with an improved model for foam generation. *SPE J.* **2007**, *12*, 35−48.

(63) Dholkawala, Z. F.; Sarma, H. K.; Kam, S. I. Application of fractional flow theory to foams in porous media. *J. Pet. Sci. Eng.* **2007**, *57*, 152−165.

(64) Myers, T. J.; Radke, C. J. Transient foam displacement in the presence of residual oil: experiment and simulation using a population-balance model. *Ind. Eng. Chem. Res.* **2000**, *39*, 2725−2741.

(65) Ma, K.; Farajzadeh, R.; Lopez-Salinas, J. L.; Miller, C. A.; Biswal, S. L.; Hirasaki, G. J. Non-uniqueness, numerical artifacts, and parameter sensitivity in simulating steady-state and transient foam flow through porous media. *Transp. Porous Media* **2014**, *102*, 325−348.

(66) Tang, J.; Vincent-Bonnieu, S.; Rossen, W. CT coreflood study of foam flow for enhanced oil recovery: The effect of oil type and saturation. *Energy* **2019**, *188*, 116022.

(67) Tang, J.; Vincent-Bonnieu, S.; Rossen, W. Experimental Investigation of the Effect of Oil on Steady-State Foam Flow in Porous Media. *SPE J.* **2019**, *24*, 140−157.